

High-Temperature Gaseous Reaction of Cesium with Siliceous Thermal Insulation: The Potential Implication to the Provenance of Enigmatic Fukushima Cesium-Bearing Material

Muhammad Rizaal,* Kunihisu Nakajima, Takumi Saito, Masahiko Osaka, and Koji Okamoto



Cite This: *ACS Omega* 2022, 7, 29326–29336



Read Online

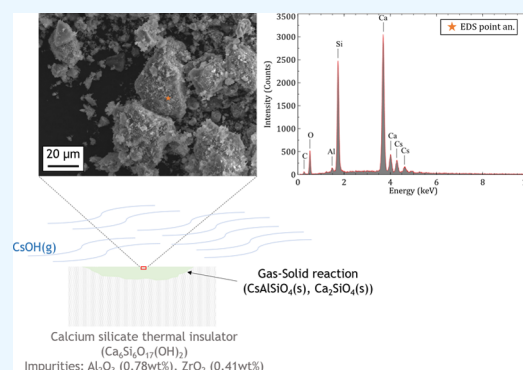
ACCESS |

Metrics & More

Article Recommendations

Supporting Information

ABSTRACT: Here, we report an investigation of the gas–solid reaction between cesium hydroxide (CsOH) and siliceous (calcium silicate) thermal insulation at high temperature, which is postulated as the origin for the formation mechanism of cesium-bearing material emitted from the Fukushima Daiichi nuclear power plant. A developed reaction furnace consisting of two heating compartments was used to study the reaction at temperatures of 873, 973, and 1073 K. Under the influence of hydrogen-steam atmospheric conditions ($H_2/H_2O = 0.2$), the reaction between cesium hydroxide vapor and solid thermal insulation was confirmed to occur at temperatures of 973 and 1073 K with the formation of dicalcium silicate (Ca_2SiO_4) and cesium aluminum silicate ($CsAlSiO_4$). Water-dissolution analyses of the reaction products have demonstrated their stability, in particular, $CsAlSiO_4$. Constituent similarity of the field-observed cesium-bearing materials near the Fukushima Daiichi nuclear power plants with $CsAlSiO_4$ suggests for the first time that gaseous reaction between CsOH with calcium silicate thermal insulation could be one of the original formation mechanisms of the cesium-bearing materials.



1. INTRODUCTION

Cesium-bearing materials or more commonly termed as CsMPs (cesium-rich microparticles) are μm -scale particles believed to be emitted from the Fukushima Daiichi nuclear power plants following the aftermath of the March 2011 severe accident.^{1,2} These particles contain highly concentrated radiocesium as reported in the first successful isolation of CsMPs by Adachi and co-workers¹ 170 km southwest of the site using aerosol samplers equipped with quartz fiber filters. The particles were characterized to have a spherical shape and consisted of Cs, Fe, Si, Zn, and other trace elements. On other occasions, CsMPs were isolated from different media, including soils,^{3–7} plant leaves or needles,^{8–10} non-woven fabric cloth used as ground cover in vegetable cultivation,^{9,10} and suspended particulate matters in rivers,¹¹ which collectively showed that such particles were heterogeneously shaped with either spherical or non-spherical shapes and consisted of various major elements. Despite their distinct forms, they were commonly classified as type-A or type-B CsMPs particles based on $^{134}\text{Cs}/^{137}\text{Cs}$ radioactivity ratios of 0.94, 1.08, and 1.05,^{2,12} which seemingly reflected their origins: units 1, 2, and 3 of the Fukushima Daiichi nuclear power plant, respectively. The type-A particles were assigned to those observed CsMPs having $^{134}\text{Cs}/^{137}\text{Cs}$ ratios similar to that of unit 2 or 3 while type-B particles were given to CsMPs with $^{134}\text{Cs}/^{137}\text{Cs}$ similar to that of unit 1. Beyond this $^{134}\text{Cs}/^{137}\text{Cs}$

ratio classification, each type of CsMPs was eventually linked to different characteristics such as structures, sizes, and major elements. Type-A CsMPs were found in spherical and non-spherical shapes with a size of 10 μm or less and made of silicate glass^{4,5,8,9} having Cs, Fe, Si, and Zn (and/or Al) in common. Although partly similar to type-A CsMPs in terms of the shapes and silicate glass structures, type-B CsMPs were found in a much larger size (>50 μm) and consisted of a heterogeneous distribution of various elements.^{4,6}

Because the CsMPs are thought to be attributed to the two major plume events in the Fukushima Daiichi nuclear power plant,¹ their formation process could provide a piece of crucial information to unveil the accident progression such as core meltdown.⁵ Considering that in such accident progressions, the formed CsMPs may not be fully ejected from the power plant but remain inside the reactor containment or reactor building, then their distribution is highly associated with the location of the original material. This means that if such a material could be understood, a well-defined approach for decommissioning

Received: June 6, 2022

Accepted: July 22, 2022

Published: August 8, 2022



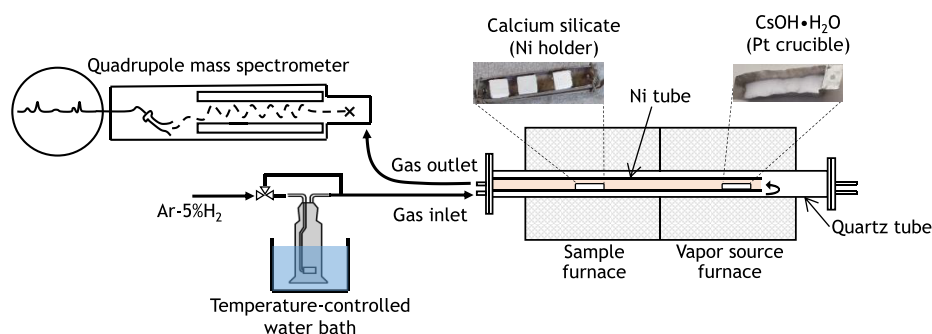


Figure 1. Schematic of the gas–solid reaction test facility.

and dismantling works in the Fukushima Daiichi nuclear power plant could be realized to protect the workers and to avoid release to the environment. To date, however, the formation process of CsMPs remains elusive, particularly the possible source of silicate. Furuki et al.⁵ suggested that the origin of SiO_2 was siliceous material contained in the concrete of pedestal structures that had been generated during molten core–concrete interaction (MCCI). Zheng et al.¹³ argued that SiO_2 originated from the volatilization of oxide scales of type-304 stainless steel material used in, e.g., control rod claddings. Martin et al.,¹⁴ based on their extensive characterization of type-B particles, proposed thermal insulating materials as the origin of such silicates, which are vastly used in the piping system of a nuclear reactor. They continued the assertion by scrutinizing the contained fiber in CsMPs, which showed a strong degree of similarity to those commonly used in thermal insulation. Martin and coworkers' hypothesis seems more plausible because a recent investigation has indicated favorable retention of cesium in thermal insulation materials through high-temperature interaction.¹⁵ Nevertheless, there is a limitation to this reported work¹⁵ due to the utilization of powdery starting materials, which could lead to the homogeneous (condensed phases) reaction. It is expected that during an accident progression, the interaction process between cesium and the suspected material occurs in the heterogeneous condition (i.e., a gas–solid reaction). Therefore to confirm the interaction process, a more practical investigation is needed.

Reflecting the above perplexity, the objective of our present study is to report, for the first time, direct evidence of heterogeneous reactions between gaseous cesium with solid siliceous (calcium silicate) thermal insulation at high temperatures, which is expected to shed light on the formation mechanism of cesium-bearing materials and eventually their provenance.

2. EXPERIMENTAL AND CALCULATION METHODS

2.1. Experiments. To study the gaseous reaction of cesium with a thermal insulation material, we employed a reaction furnace with 1000 mm in length and comprising two concentric tubes with inner diameters of 50 and 25.4 mm, respectively. The outer tube made of quartz is the passage of feed gas composed of Ar, H_2 , and H_2O to be heated up before entering the inner tube. At the inner tube made of Ni, thermal insulator samples were located 350 mm downstream from the platinum crucible containing a cesium source as depicted in Figure 1. The temperature at the samples and cesium source locations were measured in the separate blank-heating tests using K-type thermocouples. Cesium hydroxide monohydrate

(Sigma Aldrich, $\text{CsOH}\cdot\text{H}_2\text{O}$ 99.5%) and calcium silicate (Nippon Keical Limited, Keical Ace Super Silica) were used as the cesium source and the thermal insulation material, respectively. Selection of those materials was based on the following facts: (1) cesium hydroxide was regarded as the predominant form of cesium under steam in severe accident conditions,¹⁶ and (2) the main steam piping in the Fukushima Daiichi nuclear power plant was vastly equipped with calcium silicate thermal insulation.¹⁷ The Keical Ace calcium silicate insulation material consists of CaO (45.09 wt %), SiO_2 (52.3 wt %), Al_2O_3 (0.78 wt %), ZrO_2 (0.41 wt %), and other constituents with individual weight percent of less than 0.3 wt %.

Three calcium silicate samples were prepared for each test by microcutting the as-received insulation board into smaller blockish forms and were aligned in a nickel holder having a size of 60 mm (length) \times 10 mm (width). After inserting the samples and CsOH into the predetermined locations inside the Ni tube, the furnace was degassed and an atmospheric mixture of Ar/ H_2 / H_2O was then introduced by means of Ar-5% H_2 flow through a temperature-controlled water bath at 333 K and 0.1 MPa. This condition could provide a H_2 / H_2O molar ratio of ca. 0.2. The vapor source furnace with the CsOH source was ramp heated up to 893 K with a heating rate of 10.9 K/min and then brought to 923 K with a rate of 1.5 K/min before being held constant for 3 h at 923 K. Such a heating profile was employed to obtain a constant flow of CsOH as well as to prevent its rapid evaporation. The calcium silicate insulation samples were kept at three different temperatures of 873, 973, and 1073 K (i.e., performed separately) where they were chosen based on the previous thermochemical investigation.¹⁵ The study¹⁵ showed that the presence or absence of H_2O in the atmosphere could induce the formation of a similar kind of Cs compound using thermogravimetry-differential thermal analysis (TG-DTA). Hence in the present study, a steam-containing atmosphere was adopted by considering that the actual event of a nuclear severe accident would be in steam-rich conditions. The mixture of gas was fed at a constant flow rate of 100 cm^3/min , and the concentrations of hydrogen and steam were monitored at the outlet of the furnace using a quadrupole mass spectrometer (Canon Anelva Corp., M-101QA-TDM). During the cooling process of the furnace, after a 3 h holding time at target temperatures of samples and CsOH, the steam supply was shut off, leaving only Ar-5% H_2 in the gas flow. This was intended to prevent steam condensation on samples, which otherwise could alter the actual mass of deposits formed after gas–solid interaction with CsOH. The mass of deposits was calculated by subtracting the initial mass of calcium silicate samples from the final mass. Furthermore, a

Table 1. Estimated Gibbs Energy Function of Cesium Aluminosilicates ($T = 298\text{--}1200\text{ K}$)

	$G(T) - \sum_i n_i H_i^{\text{SER}} = A + BT + CT \ln T + DT^2 + ET^3 + FT^{-1}$ (J/mol)					
	A	B	C	D	E	F
CsAlSiO ₄	-2.207×10^6	8.361×10^2	-1.447×10^2	-1.682×10^{-2}	0	1.470×10^6
CsAlSi ₂ O ₆	-3.161×10^6	1.214×10^3	-2.068×10^2	-2.232×10^{-2}	0	2.100×10^6
CsAlSi ₅ O ₁₂	-6.007×10^6	2.086×10^3	-3.481×10^2	-6.796×10^{-2}	0	3.990×10^6

Table 2. Measurements of Samples and CsOH before and after Gas-Solid Reaction Tests

group of tests	T (K)	before gas–solid reaction tests			after gas–solid reaction tests					
		samples, m_{s0} (g)	samples, V_0 ($w \times l \times t$) (mm)	CsOH, m_{c0} (g)	samples, m_{s1} (g)	samples, V_1 ($w \times l \times t$) (mm)	mass difference, $m_{s1} - m_{s0}$ (g)	$\frac{m_{s1} - m_{s0}}{m_{s0}}$ (%)	$\frac{V_1 - V_0}{V_0}$ (%)	CsOH, m_{c1} (g)
1-1	1073	0.0579	$7.2 \times 7.8 \times 3.1$	3.4803	0.1068	$2.6 \times 3.5 \times 1.1$	0.0489	85	−94	3.1278
1-2	1073	0.0666	$7.5 \times 7.6 \times 3.1$		0.1157	$3.8 \times 4.2 \times 1.8$	0.0491	74	−84	
1-3	1073	0.0640	$6.3 \times 8.9 \times 3.8$		0.1090	$2.9 \times 4.6 \times 1.6$	0.0450	70	−90	
2-1	973	0.0734	$7.3 \times 8.4 \times 3.5$	3.9336	0.1066	$7.0 \times 8.0 \times 3.0$	0.0332	45	−21	2.7135
2-2	973	0.0588	$6.1 \times 7.8 \times 3.4$		0.0911	$5.6 \times 7.2 \times 2.7$	0.0323	55	−33	
2-3	973	0.0577	$6.2 \times 7.5 \times 3.4$		0.1031	$5.4 \times 6.1 \times 2.4$	0.0454	79	−50	
3-1	873	0.0610	$5.8 \times 7.1 \times 3.7$	3.5114	0.1332	$5.0 \times 6.9 \times 1.5$	0.0722	118	−66	2.9702
3-2	873	0.0578	$5.6 \times 8.0 \times 3.0$		0.1352	$3.5 \times 7.2 \times 0.4$	0.0774	134	−92	
3-3	873	0.0648	$7.0 \times 7.8 \times 3.0$		0.1965	$5.0 \times 5.1 \times 1.6$	0.1317	203	−75	

ratio between the mass of deposits and the initial mass of calcium silicate could serve not only as the capacity of thermal insulation to retain cesium at high temperatures but also as an indication of the occurrence of a gas–solid reaction. Therefore, the post-test mass and dimension measurements were carefully taken inside the nitrogen inert glovebox with a moisture content of a few ppm to preserve the samples against moisture absorption. After recording such information, samples were pulverized using an agate mortar and pestle and then subjected to post-test analyses.

2.2. Post-test Analyses. The pulverized samples were first dissolved with water before their post-test analyses to mitigate the adverse effect of the condensed CsOH. This is because we encountered large moisture absorption in the previous work,¹⁵ which caused the chemical phase identification to be difficult. The dissolution process is as follows: each sample was initially submerged for 72 h in the designated polypropylene tubes containing 20 mL of deionized water and then separated from the supernatant for drying on a ceramic hot plate with a temperature of 383 K. To confirm the adequacy of this process, the 1073 K samples were used and the chemical phase (before and after the treatment) was analyzed using powder X-ray diffractometry (PXRD) (Figure S1). This procedure, in addition to the original intention for removing condensed CsOH, turned out to be able to unveil whether the formed cesium compounds after a gaseous CsOH–solid siliceous thermal insulation reaction are water-soluble or water-insoluble. The solubility of reaction products is important because it could provide a quick grasp of the fate of radiologically important reaction products such as cesium, whether it could remain (insoluble) or could be removed from host material (soluble) that is likely to redistribute further. The cesium phases that could be identified in the final PXRD analysis are classified as insoluble cesium; otherwise, they are classified as soluble cesium. Next, the rest of the samples (873 and 973 K) underwent a similar water dissolution process and were analyzed in their final condition.

A scanning electron microscope equipped with an energy-dispersive X-ray spectrometer (SEM/EDS–silicon drift detector, JSM-IT100, JEOL) was applied to the water-dissolved samples for microstructure and spatial elemental distribution analyses. Double-sided carbon tape was affixed to the sample holder (Al) to place samples without any further coating. The secondary electron images were obtained at 15 kV. For the phase identification of the samples, PXRD analyses with a Rigaku MiniFlex600SC (Cu $K\alpha$ radiation) were carried out at room temperature in an air-tight sample holder. The diffraction analysis was performed over the scan range 2θ of $10\text{--}60^\circ$ in continuous mode with a step size of 0.01° and scanning speed of $2^\circ/\text{min}$ at the applied voltage and current of 40 kV and 15 mA, respectively.

2.3. Thermodynamic Calculation. To further investigate the reaction involving the Cs–Ca–Al–Si–O–H system, we employed thermodynamic equilibrium calculation using a Thermo-Calc 2021a¹⁸ with SGTE (Scientific Group Thermodynamic data Europe) substance database version 5 to predict the stable species of cesium. In the database, however, only cesium silicates (i.e., Cs₂SiO₃, Cs₂Si₂O₅, and Cs₂Si₄O₉) are available; thus, it is not possible to gain a comprehensive understanding of where cesium aluminosilicates are potentially formed. Therefore, as a first step, we modified the SGTE database of a Cs–Ca–Al–Si–O–H system by incorporating the cesium aluminosilicates. We introduced three cesium aluminosilicates, i.e., CsAlSiO₄, CsAlSi₂O₆, and CsAlSi₅O₁₂, that had been reported in the literature regarding their thermodynamic properties,^{19–22} through the Gibbs energy function based on the following SGTE format:

$$G(T) - \sum_i n_i H_i^{\text{SER}} = A + BT + CT \ln T + DT^2 + ET^3 + FT^{-1} \quad (1)$$

where n_i and H_i^{SER} represent the number of atoms and the standard reference enthalpy for each element i in the cesium aluminosilicates, respectively. The polynomial coefficients for

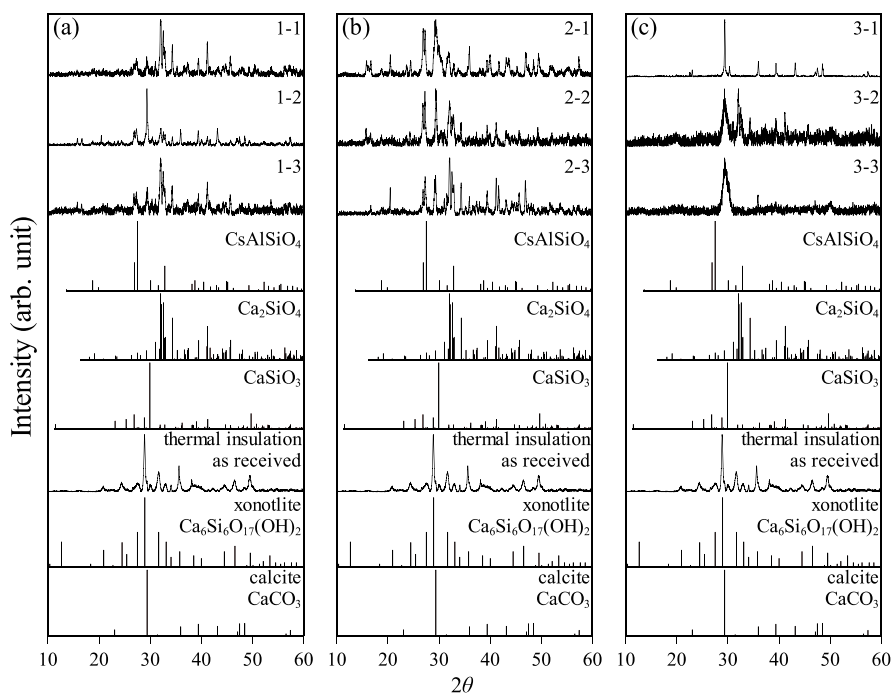


Figure 2. XRD results of water-dissolved samples: (a) group 1 (1073 K), (b) group 2 (973 K), and (c) group 3 (873 K). ICDD card nos. 31-0386 (CsAlSiO₄), 80-8935 (Ca₂SiO₄), 66-0271 (CaSiO₃), 23-0125 (Ca₆Si₆O₁₇(OH)₂), and 78-4615 (CaCO₃).

CsAlSiO₄, CsAlSi₂O₆, and CsAlSi₅O₁₂ were derived in the temperature range of 298–1200 K using the estimated heat capacity functions $C_p(T)$, standard enthalpy formation $\Delta_f H^\circ_{298}$, and standard entropy S°_{298} reported by Yui et al.¹⁹ Table 1 lists the coefficients for each cesium aluminosilicate.

In the first half of thermodynamic equilibrium calculations, the input parameters of reaction temperatures and pressure were set in the range of 673–1173 K and 0.1 MPa, respectively, while the amount of each element (in mole fraction) was thoroughly determined based on the experimental conditions (i.e., CsOH vapor, H₂/H₂O ratio, and calcium silicate samples) and also on the condition with low steam partial pressure for the sake of phase stability examination. In the second half of the calculations, with the emphasis on cesium abundance (Cs/(Al + Si)), the stable species were examined in an increasing total pressure to foresee them in the event of a nuclear severe accident.

3. RESULTS AND DISCUSSION

3.1. Mass and Size Changes. Table 2 lists the size and mass information of the thermal insulation material before and after experiments at the respective temperatures. We noted that almost all samples experienced shrinkage ($(V_1 - V_0)/V_0 < 0$) but exhibited increases in their masses ($m_{s1} - m_{s0}$). The magnitude of shrinkage varied between 21 and 94%, and the largest one occurred in the 1073 K test. To be more precise, if we consider only a linear shrinkage, for instance, sample 2-1 whose magnitude of linear shrinkage (thickness change) of 14% is much greater than the industry-claimed linear shrinkage of 2% at 1273 K and 3 h test (i.e., Keical Ace Super Silica of Nippon Keical Ltd). The 2% shrinkage, considering the crystal structure of the thermal insulation as xonotlite, is consistent with the minute change of xonotlite after dehydration observed by Dent and Taylor.²³ They found that the final crystal structure was transformed into low-temperature wollastonite (β -CaSiO₃), which had a higher density of 2.75 g/cm³ than

that of xonotlite, 2.71 g/cm³. Therefore, in our study, the shrinkage could not be straightforwardly seen as a result of water molecule or hydroxyl group removal alone; instead, it should reflect crystal transformation caused by a reaction with cesium. This is because all samples showed large mass increases after the tests, which are indicative of the coexistence of cesium in thermal insulation.

At 973 K (group 2) and 1073 K (group 1), the reaction was expected to prevail in the gas–solid interface by considering that at these temperatures, CsOH could be kept in vapor condition due to greater vapor pressure than that in the original/source location (at 923 K). On the other hand, at 873 K (group 3), the reaction was expected to occur in the condensed phase reaction due to lower vapor pressure. The corresponding vapor pressure of CsOH was calculated using thermodynamic data of CsOH (g) and CsOH (s,l) reported by Cordfunke and Konings²⁴ in the temperature range of 615.5–1300 K in the following equation:

$$\log p(\text{atm}) = -\frac{8561.51}{T} - 5.18 \log T + 3.38 \times 10^{-4} T + 22.14 \quad (2)$$

Supposing that a homogeneous temperature was attained at each group of the tests, then the estimated CsOH vapor pressures at the sample location would be 6.53×10^{-2} (group 1), 1.52×10^{-2} (group 2), and 2.42×10^{-3} atm (group 3), while the vapor pressure in the source location was estimated to be 6.40×10^{-3} atm. The calculated vapor pressures show that the first two groups have positive pressure differences of 5.89×10^{-2} and 8.78×10^{-3} atm, respectively, as compared to the source location, which are considered important to preserving CsOH in the vapor phase. This indicates that the measured increase in the masses of the thermal insulation materials was not affected by condensation of CsOH, but instead, by the results of gas–solid reactions. Contrarily, due to

Table 3. Quantitative Analysis of Calcium Silicate Thermal Insulation

sample/ temperature (K)	phases (wt %) ^a	molar ratio [–]	formation mechanism of new phases
as-received	Ca ₆ Si ₆ O ₁₇ (OH) ₂ (87.6), CaCO ₃ (12.4)		
1-1/1073	CaCO ₃ (5.1), CaSiO₃ (17.4) , CsAlSiO₄ (7.0) , Ca₂SiO₄ (70.5)	CsAlSiO ₄ /Ca ₂ SiO ₄ = 0.07	dehydration of xonotlite (eq 3) Ca ₆ Si ₆ O ₁₇ (OH) ₂ (s) = 6CaSiO ₃ (s) + H ₂ O(g) Δ _r G° (900 K) = –188.67 kJ/mol
1-2/1073	CaCO ₃ (41.7), CaSiO₃ (15.9) , CsAlSiO₄ (10.9) , Ca₂SiO₄ (31.5)	CsAlSiO ₄ /Ca ₂ SiO ₄ = 0.24	
1-3/1073	CaCO ₃ (12.7), CaSiO₃ (16.2) , CsAlSiO₄ (9.3) , Ca₂SiO₄ (61.8)	CsAlSiO ₄ /Ca ₂ SiO ₄ = 0.10	reaction with CsOH (eq 4) 4CaSiO ₃ (s) + Al ₂ O ₃ (s) + 2CsOH(g) = 2CsAlSiO ₄ (s) + 2Ca ₂ SiO ₄ (s) + H ₂ O(g) Δ _r G° (973 – 1073 K) = – 254.38 – –228.75 kJ/mol
2-1/973	Ca ₆ Si ₆ O ₁₇ (OH) ₂ (24.6), CaCO ₃ (23.1), CsAlSiO₄ (12.6) , Ca₂SiO₄ (39.7)	CsAlSiO ₄ /Ca ₂ SiO ₄ = 0.22	
2-2/973	CaCO ₃ (26.6), CaSiO₃ (19.8) , CsAlSiO₄ (12.9) , Ca₂SiO₄ (40.7)	CsAlSiO ₄ /Ca ₂ SiO ₄ = 0.22	reaction with CsOH (eq 5) 2CaSiO ₃ (s) + 2CsOH(g) = Cs ₂ SiO ₃ (s) + Ca ₂ SiO ₄ (s) + H ₂ O(g) Δ _r G° (973–1073 K) = –150.22 – –163.05 kJ/mol
2-3/973	Ca ₆ Si ₆ O ₁₇ (OH) ₂ (12.9), CaCO ₃ (11.4), CaSiO₃ (19.8) , CsAlSiO₄ (9.9) , Ca₂SiO₄ (65.8)	CsAlSiO ₄ /Ca ₂ SiO ₄ = 0.10	
3-1/873	Ca ₆ Si ₆ O ₁₇ (OH) ₂ (13.3), CaCO ₃ (86.7)	–	reaction with CsOH (eq 6) Ca ₆ Si ₆ O ₁₇ (OH) ₂ (s) + 6CsOH(l) = 3Cs ₂ SiO ₃ (s) + 3Ca ₂ SiO ₄ (s) + 4H ₂ O(g) Δ _r G° (873 K) = –447.47 kJ/mol
3-2/873	Ca ₆ Si ₆ O ₁₇ (OH) ₂ (13.0), CaCO ₃ (37.3), Ca₂SiO₄ (49.7)	–	
3-3/873	Ca ₆ Si ₆ O ₁₇ (OH) ₂ (14.2), CaCO ₃ (85.8)	–	

^aThe newly formed phases are shown in bold-typed texts

the negative vapor pressure difference of -3.99×10^{-3} atm, the measured mass of thermal insulation in group 3 was likely affected by the condensation of CsOH, which therefore could not simply suggest the generated amount of product after the condensed phase reaction. In groups 1 and 2, there were average values of 0.0477 and 0.0370 g of the mass increase. Meanwhile, as expected, we found that the mass increase in group 3 was the largest among the group of tests with a value in the range of 0.0722–0.1317 g. This information would be physicochemically meaningful if they are corrected to the initial mass of thermal insulation, as stressed in the latter Section 2.1. The parameter, a ratio between mass of the deposit (or mass change) and the initial mass of thermal insulation, denoted as $(m_{s1} - m_{s0})/m_{s0}$ in Table 2, could provide the information on the capacity of the original calcium silicate material to retain cesium at high temperature and also as an indication for the occurrence of the reaction. If such a presumption is valid, one should obtain a common ratio in both groups 1 and 2. The practically identical samples in these groups, in terms of initial mass, are samples 1-1 and 2-3 (intergroup) and samples 1-2 and 1-3 (intragroup). We found that in intragroup comparison, i.e., the same temperature and initial mass, the ratio was approximately $72 \pm 2\%$ while the intergroup counterpart had a ratio of $82 \pm 3\%$. Further, the individual shrinkage for these samples showed a ratio above 50%. Therefore, it could be approximated that the cesium retention capacity of the thermal insulation material above 70% could be used as indirect information on the occurrence of gas–solid reaction when combined with the shrinkage factor of greater than 50%. Otherwise, confirmatory analyses are needed such as for samples 2-1 and 2-2, which possessed a lower shrinkage factor and mass capacity ratio. For group 3, the capacity ratio was much larger than the former groups due to the influences from CsOH condensation. Consequently, it is difficult to indirectly determine whether the reaction had taken place.

3.2. Composition and Morphology. To further investigate, we analyzed the crystal phases of the samples from all groups of tests including the as-received calcium silicate thermal insulation using PXRD. The obtained profiles were

baseline-corrected and compared with the ICDD database for identification as shown in Figure 2. After the phase identification, an X-ray diffraction quantitative analysis was performed on each sample using the Rietveld refinement method in Profex 4.3.5²⁵ and listed in Table 3. The as-received thermal insulation was found to largely consist of xonotlite (Ca₆Si₆O₁₇(OH)₂) with calcite (CaCO₃) as a minor phase. This type of xonotlite-based calcium silicate structure is thermally stable up to the temperature of ca. 1073 K^{15,23,26} before undergoing crystal transformation into wollastonite (CaSiO₃). In this study, however, with the presence of cesium in the system, such an ideal transformation accompanied by the release of water molecules or hydroxyl groups (Ca₆Si₆O₁₇(OH)₂ → 6CaSiO₃ + H₂O) was restricted; instead, some additional new crystal phases were obtained. Cesium aluminum silicate (CsAlSiO₄) and dicalcium silicate (Ca₂SiO₄) were identified in the samples 1-1, 1-2, and 1-3 of group 1, samples 2-1, 2-2, and 2-3 of group 2, and sample 3-2 of group 3. An exception is sample 3-2, where dicalcium silicate was identified without cesium aluminum silicate. This anomaly could be explained as the consequence of condensed phase reactions prevailing only in group 3 that led to a different reaction path having no CsAlSiO₄ in the final product. Such selectivity is analogous to the case of Al exclusion from the reaction system,¹⁵ which solely yielded Ca₂SiO₄. The theoretical approach suggested that a cesium silicate compound Cs₂SiO₃ (water-soluble) was thermodynamically favorable to form along with Ca₂SiO₄, while its identification remained unclear.¹⁵ The rest of the samples in group 3 showed no formation of new phases, but their predominant crystal structure had changed into calcite. It is considered that this structural alteration was caused by the partial reaction attributed to the formation of Cs₂SiO₃ and Ca₂SiO₄ (see Table 3, formation mechanism). The main reaction is described as a two-stage process where xonotlite initially reacts with CsOH to form Cs₂SiO₃ (i.e., Ca₆Si₆O₁₇(OH)₂(s) + 12CsOH(l) = 6Cs₂SiO₃(s) + 6CaO(s) + 7H₂O(g)) and then the remaining xonotlite in the bulk of thermal insulation interacts with the first-stage reaction product calcium oxide to form Ca₂SiO₄ (i.e., Ca₆Si₆O₁₇(OH)₂(s) + 6CaO(s) =

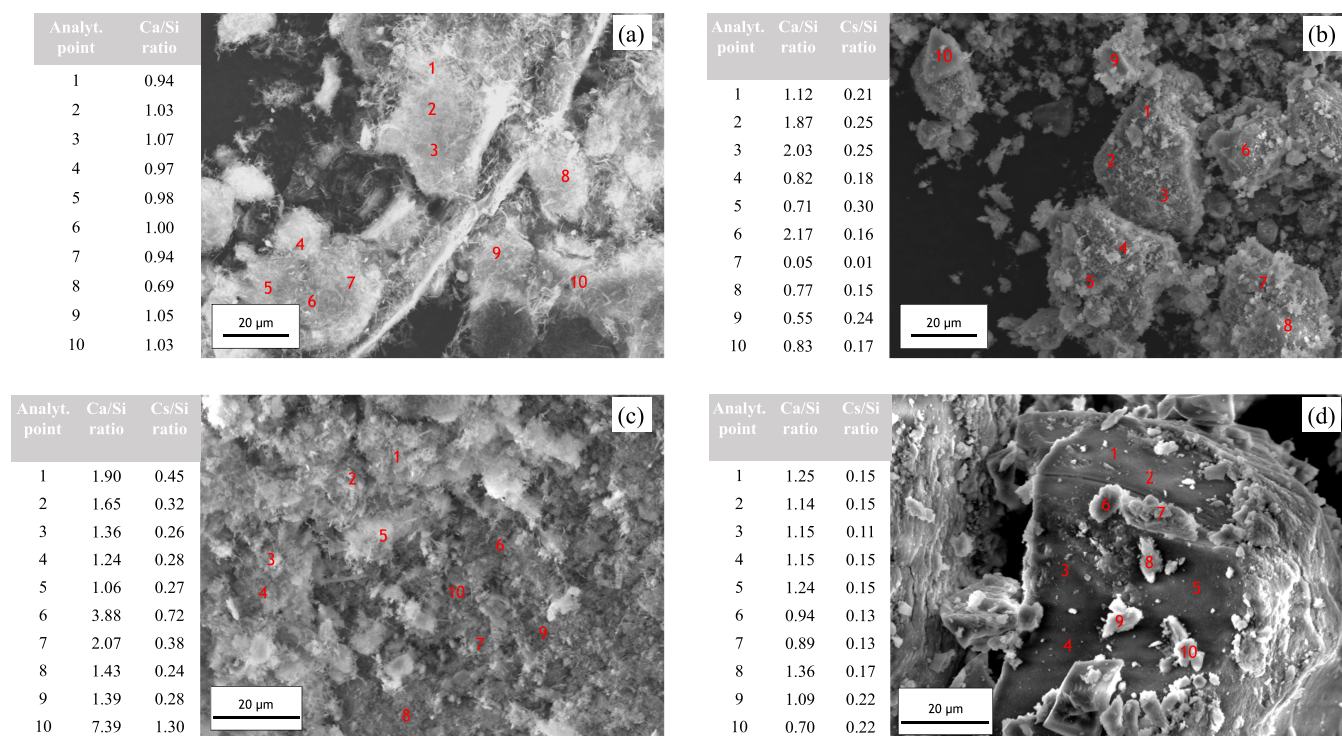


Figure 3. Secondary electron images of calcium silicate thermal insulation: (a) as-received, (b) sample 1-2/1073 K test, (c) sample 2-1/973 K test, and (d) sample 3-2/873 K test. The numbers indicate quantitative point analyses.

$6\text{Ca}_2\text{SiO}_4(\text{s}) + \text{H}_2\text{O}(\text{g})$). If the latter formation did not proceed to completion, calcium oxide could readily react with CO_2 contained in an air atmosphere (e.g., during sample handling) to form CaCO_3 . Based on these results of the PXRD analysis, it can be confirmed that the gas–solid reaction occurred between cesium and thermal insulation (groups 1 and 2) and to a lesser extent in the condensed phase (group 3), which are in agreement with the predicted thermal analyses in our previous study.¹⁵

Despite its low content (0.78 wt %), aluminum impurity in thermal insulation material had proven to be crucial to yield interaction with cesium in a gas–solid reaction system by forming the cesium aluminum silicate (CsAlSiO_4). This might be attributed to the aluminum coordination in calcium silicate layers of the xonotlite structure, where it is arguably to be located in the bridging site (i.e., connected with two other silicate tetrahedra chains) upon its isomorphic substitution of silicon atom,^{27–29} hence favoring aluminosilicate $[\text{AlSiO}_4]^-$ bonds with foreign cationic ions. The CsAlSiO_4 compound is expected to be formed together with dicalcium silicate (Ca_2SiO_4) when the reaction could proceed to completion, based on an analogous two-stage process of Cs_2SiO_3 – Ca_2SiO_4 formation described above. According to the results of quantitative analysis, we could calculate the molar ratio of these two compounds. It was found that their molar ratios (Table 3) were generally less than 0.25, which is far from unity if we consider an ideal reaction in eq 4. In other words, the reaction system had produced more dicalcium silicate using not only reaction in eq 4 but also different reaction paths such as reaction in eq 5.¹⁵ It should be emphasized that, although a single formation of Ca_2SiO_4 is possible at a higher Ca/Si ratio such as in hillebrandite,^{26,30} it is unlikely in our experimental condition where the Ca/Si ratio is one. This means that by taking into account the contribution of Ca_2SiO_4 content also

from the reaction in eq 5, a discrepancy of the $\text{CsAlSiO}_4/\text{Ca}_2\text{SiO}_4$ ratio from unity was justified.

The Cs_2SiO_3 phase, on the other hand, as the consequence of reaction in eq 5, could not be confirmed through PXRD prior to the dissolution process (Figure S1), which was considered to be caused by its amorphous structure.¹⁵ Nevertheless, a separate study using the developed quantification method on inductively coupled plasma optical emission spectroscopy (ICP-OES) has succeeded to unveil this Cs compound³¹ by indirect determination of soluble Cs and Si. The developed method is initially tested on an artificial solution with a known solute concentration of Cs and Si, and the findings are compared with similar quantification using conventional methods to confirm whether the measured Cs concentrations have not suffered from the ionization interference. Afterward, the method is applied to determine Cs and Si concentration in the solutions that were previously used to dissolve samples of the cesium–calcium silicate gas–solid reaction test. The results show that all solutions from the 1073 and 973 K tests have an approximately Cs/Si molar ratio of 2, while those of the 873 K test indicate greater ratios.³¹ It is worth noting that cesium silicate compounds in the pseudo-binary phase diagram of Cs_2O – SiO_2 comprise $\text{Cs}_2\text{Si}_4\text{O}_9$, $\text{Cs}_2\text{Si}_2\text{O}_5$, Cs_2SiO_3 or its trimer $\text{Cs}_6\text{Si}_3\text{O}_9$, and $\text{Cs}_6\text{Si}_2\text{O}_7$,^{32–34} which correspond to the Cs/Si molar ratio of 0.5, 1, 2, and 3, respectively. In other words, when a dissolution process had been applied to each of these cesium silicates, one should obtain approximate dissolved concentrations of Cs over Si to be relevant to its original silicate compound; otherwise, there is a coexistence of different Cs-containing materials such as CsOH at the 873 K test. To this end, the study³¹ has corroborated that the Cs_2SiO_3 phase is unequivocally formed during the gas–solid reaction of cesium and calcium silicate thermal insulation. Furthermore, the thermodynamic analyses

Table 4. Input Parameters for Thermodynamic Evaluation ($T = 673\text{--}1173\text{ K}$)

	case 1 ^a /case 7 ^b ($\text{H}_2/\text{H}_2\text{O} = 0.20$) ($\text{Cs}/(\text{Al} + \text{Si}) = 2.75$)	case 2 ($\text{H}_2/\text{H}_2\text{O} = 0.20$) ($\text{Cs}/(\text{Al} + \text{Si}) = 5.51 \times 10^{-2}$)	case 3 ($\text{H}_2/\text{H}_2\text{O} = 0.20$) ($\text{Cs}/(\text{Al} + \text{Si}) = 2.75 \times 10^{-2}$)	case 4/case 8 ^c ($\text{H}_2/\text{H}_2\text{O} = 100$) ($\text{Cs}/(\text{Al} + \text{Si}) = 2.75$)	case 5 ($\text{H}_2/\text{H}_2\text{O} = 100$) ($\text{Cs}/(\text{Al} + \text{Si}) = 5.51 \times 10^{-2}$)	case 6 ($\text{H}_2/\text{H}_2\text{O} = 100$) ($\text{Cs}/(\text{Al} + \text{Si}) = 2.75 \times 10^{-2}$)
Cs (mole fraction)	2.43×10^{-3}	4.89×10^{-5}	2.43×10^{-5}	2.43×10^{-3}	4.89×10^{-5}	2.43×10^{-5}
O (mole fraction)	2.96×10^{-1}	2.96×10^{-1}	2.96×10^{-1}	1.01×10^{-2}	7.74×10^{-3}	7.70×10^{-3}
H (mole fraction)	7.00×10^{-1}	7.03×10^{-1}	7.03×10^{-1}	9.86×10^{-1}	9.90×10^{-1}	9.90×10^{-1}
Ca (mole fraction)	8.70×10^{-4}	8.70×10^{-4}	8.70×10^{-4}	8.70×10^{-4}	8.70×10^{-4}	8.70×10^{-4}
Si (mole fraction)	8.70×10^{-4}	8.70×10^{-4}	8.70×10^{-4}	8.70×10^{-4}	8.70×10^{-4}	8.70×10^{-4}
Al (mole fraction)	1.60×10^{-5}	1.60×10^{-5}	1.60×10^{-5}	1.60×10^{-5}	1.60×10^{-5}	1.60×10^{-5}
system size (mol)	1.79	1.79	1.79	1.79	1.79	1.79
pressure (MPa)	0.1/0.1–0.7	0.1	0.1	0.1/0.1–0.7	0.1	0.1

^aRepresentation of our experimental condition with $\text{H}_2/\text{H}_2\text{O} = 0.20$, $\text{Cs}/(\text{Al} + \text{Si}) = 2.75$, and $P = 0.1\text{ MPa}$. ^bExtrapolated case in an increasing pressure with the high steam partial pressure and high cesium abundance. ^cExtrapolated case in an increasing pressure with the low steam partial pressure and high cesium abundance.

provided in Section 3.3 also support this inference where the abundance of Ca_2SiO_4 (i.e., PXRD quantification) indeed originated from Cs_2SiO_3 formation.

Figure 3 presents the SEM/EDS results on the as-received materials and the selected water-dissolved samples from each group of tests. The as-received calcium silicate thermal insulation was observed to consist of particles with acicular shapes having a Ca/Si ratio of ca. 1.0, which is a typical xonotlite structure.^{35–37} This agrees well with the identified xonotlite phase in the X-ray diffraction analysis. Meanwhile, after the high-temperature gas–solid interaction test, the samples showed morphological changes with wide-range Ca/Si ratios. In samples 1-2 (1073 K test) and 2-1 (973 K test), some analytical points indicated that Ca became enriched with a Ca/Si ratio of ca. 2.0, suggesting the presence of the Ca_2SiO_4 phase. However, we could also find that the Ca/Si ratio in sample 2-1 far exceeded this value at points 6 and 10. This could be caused by the presence of another Ca-rich phase like CaCO_3 along with the Ca_2SiO_4 phase, as what had been identified in XRD. In sample 3-2 (873 K test), the quantitative analysis did not show highly Ca-enriched particles as that in the former two tests, where the Ca/Si ratio was 1.09 on average. It is considered that the Si in such quantification was not only from Ca_2SiO_4 and unreacted $\text{Ca}_6\text{Si}_6\text{O}_{17}(\text{OH})_2$ but also from Cs_2SiO_3 that remained in sample 3-2, as represented by spatial element mapping (Figure S2) having Cs–Si–O congruency. The quantitative analysis showed that the Cs/Si molar ratios were in the range of 0.11–0.22 (Figure 3d). Concerning the Al-containing compound CsAlSiO_4 , (i.e. confirmed to be formed at 1073 and 973 K by XRD), we obtained a good spatial distribution of its elements only at certain EDS mapping areas as in sample 1-2 (Figure S2), which could be caused by its low concentration as compared to the rest of identified phases in XRD (Ca_2SiO_4 , CaSiO_3 or $\text{Ca}_6\text{Si}_6\text{O}_{17}(\text{OH})_2$, and CaCO_3). For details, if we consider the phase contribution conforms to the bulk quantitative XRD, i.e., sample 1-2 (41.7 wt % CaCO_3 , 15.9 wt % CaSiO_3 , 10.9 wt % CsAlSiO_4 , 31.5 wt % Ca_2SiO_4) and sample 2-1 (23.1 wt % CaCO_3 , 24.6 wt % $\text{Ca}_6\text{Si}_6\text{O}_{17}(\text{OH})_2$, 12.6 wt % CsAlSiO_4 , 39.7

wt % Ca_2SiO_4), a conservative calculation would result in 0.12 and 0.16 of Cs/Si molar ratio in samples 1-2 and 2-1, respectively. Therefore, it is justified that such low molar ratios, and hence yielding fair Cs–Al spatial distributions, are caused by major influences from other phases. In spite of that, the conservative ratios (0.12 and 0.16) were satisfied in each sample (Figure 3b,c), corroborating the presence of the CsAlSiO_4 phase.

3.3. Thermodynamic Stability of Cs–(Al)–Si–O Phases. In the thermodynamic evaluation, 8 cases were analyzed by adjusting the variables: hydrogen to steam ratio, the abundance of cesium ($\text{Cs}/(\text{Al} + \text{Si})$), and total pressure. Table 4 summarizes the input parameters for each case. Case 1 is a simulated case for our experimental condition where the mole fractions of elements were derived as follows: Ca, Si, and Al mole fractions were determined by summation of the mass of three calcium silicate samples, averaging them with each group of tests (Table 2), multiplying with weight fraction based on constituents in Keical Ace thermal insulation (i.e., 0.9740 for Ca and Si, 0.0078 for Al), and correcting the results with the molecular weight of xonotlite ($\text{Ca}_6\text{Si}_6\text{O}_{17}(\text{OH})_2$) and Al_2O_3 , respectively; the Cs mole fraction was obtained by averaging the mass of evaporated CsOH for all group of tests (i.e., 0.5641 g) and correcting it with the molecular weight of CsOH; H and O mole fractions were collectively determined from the amount of gas flow (steam and hydrogen), xonotlite, Al_2O_3 , and CsOH, respectively. Concerning the amount of gas flow, it was approximated by the equation of state starting from the room temperature at the upstream of test apparatus, 923 K on the top of CsOH crucible, and at last the temperature on the top of samples for 3 h (here, 1073 K was chosen for simplification). The remaining seven cases were analyzed for scrutinizing the stability of cesium species in (1) high steam partial pressure but low cesium abundance at standard atmospheric pressure (cases 2 and 3), (2) low steam partial pressure but high cesium abundance at standard atmospheric pressure (case 4), (3) low steam partial pressure and low cesium abundance at standard atmospheric pressure (cases 5 and 6), (4) high steam partial pressure and high cesium

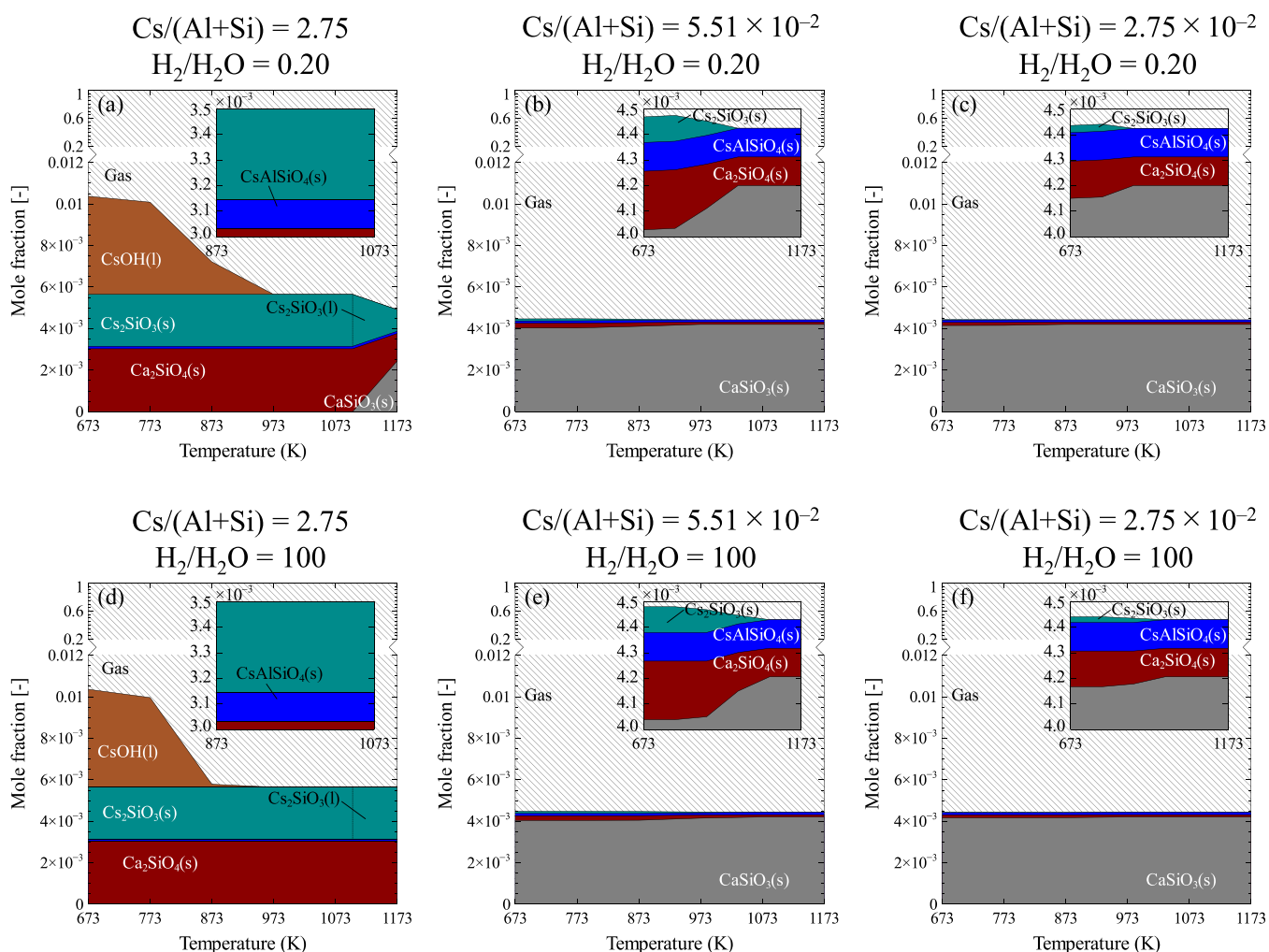


Figure 4. Thermodynamic equilibrium-based temperature-dependent species of Cs, Ca, Al, and Si in (a) case 1, (b) case 2, (c) case 3, (d) case 4, (e) case 5, and (f) case 6. See text for details of each case. The insets depict cesium (alumino)silicates on $T = 673\text{--}1173$ K or $873\text{--}1073$ K.

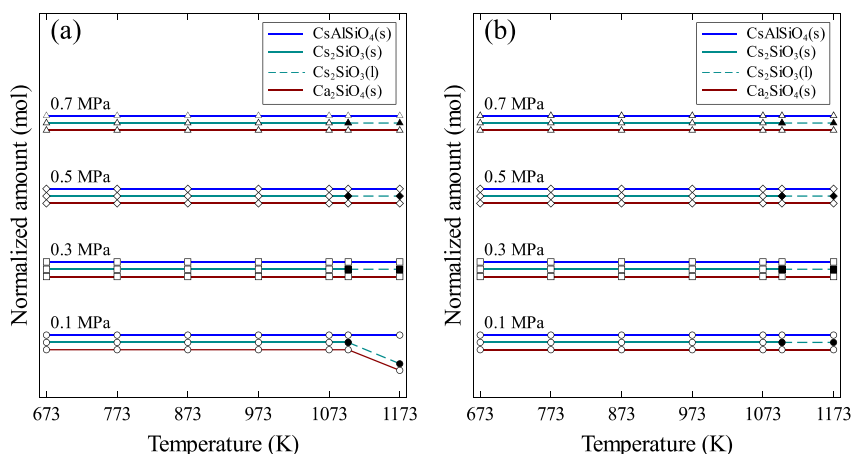


Figure 5. Isobaric temperature-dependent amount of $\text{CsAlSiO}_4(\text{s})$, $\text{Cs}_2\text{SiO}_3(\text{s,l})$, and $\text{Ca}_2\text{SiO}_4(\text{s})$ in (a) case 7 and (b) case 8.

abundance at an increasing pressure (case 7), and (5) low steam partial pressure but high cesium abundance at an increasing pressure (case 8).

The predominance diagram in Figure 4 presents the predicted species of Cs, Ca, Al, and Si in condensed phases as a function of temperature based on the respective input parameters in Table 4. In the diagrams, $\text{Cs}_2\text{SiO}_3(\text{s})$,

$\text{Cs}_2\text{SiO}_3(\text{l})$, $\text{CsAlSiO}_4(\text{s})$, and $\text{Ca}_2\text{SiO}_4(\text{s})$ are predicted to be the stable species in both low and high steam partial pressure above 873 K (Figure 4a,d). These results excellently agree with the experimentally observed water-insoluble phases in our study (i.e., $\text{CsAlSiO}_4(\text{s})$ and $\text{Ca}_2\text{SiO}_4(\text{s})$), which infers the appropriateness of our modified database through the incorporation of all cesium aluminosilicates in the calculations

(elucidated in Section 2.3). However, it should be highlighted that those phases were identified in the experiment at 873–1073 K for $\text{Ca}_2\text{SiO}_4(\text{s})$ and 973–1073 K for $\text{CsAlSiO}_4(\text{s})$. This is considered that at a lower temperature (<973 K), the formation of $\text{CsAlSiO}_4(\text{s})$ necessitates a much longer equilibration time, which had not been satisfied in our experiment. This might be attributed to a different mode of reaction, i.e., condensed CsOH reaction with solid calcium silicate rather than gas–solid reaction, which depends on the degree of CsOH diffusion/penetration from the surface of calcium silicate sample. Consequently, it could limit the reaction yield with the fractional Al contained in silicate layers in the thermal insulation. Nevertheless, the calculations could foresee the Cs species quite well and particularly $\text{CsAlSiO}_4(\text{s})$ as the most stable cesium in the reaction system of Cs–Ca–Al–Si–O–H regardless of cesium abundance or steam partial pressure (Figure 4a–f). Furthermore, $\text{CsAlSiO}_4(\text{s})$ was not singly formed in the system; instead, it was concurrently formed with $\text{Ca}_2\text{SiO}_4(\text{s})$. This can be deduced from the equivalent distribution of both species in the less Cs abundance conditions (Figure 4b,c,e,f), which is ca. 1.12×10^{-4} mole fraction. In other words, the presumed two-stage reaction process having cesium aluminum silicate ($\text{CsAlSiO}_4(\text{s})$) and dicalcium silicate ($\text{Ca}_2\text{SiO}_4(\text{s})$) in the final products has been corroborated by this thermodynamic calculation. Additionally, at higher total pressure, $\text{CsAlSiO}_4(\text{s})$ prevailed with its stability regardless of the steam partial pressure (Figure 5a,b).

$\text{Cs}_2\text{SiO}_3(\text{s})$ emerged as another stable phase in high cesium abundance conditions (Figure 4a,d) as well as to the least extent in moderate abundance ones (Figure 4b,c,e,f). In the former conditions, $\text{Cs}_2\text{SiO}_3(\text{s})$ was predicted to be stably formed in all temperature ranges of calculation while the latter conditions indicated its formation occurred in the temperature of less than 973 K. The results showed that this phase in the high cesium abundance cases was relatively higher than the $\text{CsAlSiO}_4(\text{s})$, i.e. approx. 2.50×10^{-3} mole fraction, which implies the favorability of the Cs–Si–O reaction. This turned out to pose a major role in a large formation of $\text{Ca}_2\text{SiO}_4(\text{s})$ particularly in low steam partial pressure conditions (Figure 4d). In high steam partial pressure and high-temperature conditions (i.e., $\text{H}_2/\text{H}_2\text{O} = 0.2$; $T > 1073$ K), however, the $\text{Cs}_2\text{SiO}_3(\text{s,l})$ amount was reduced and coincided with the increase of CaSiO_3 and gaseous Cs. It is because, above its melting temperature (1100 K³²), the dissociation into atomic Cs, O_2 , and SiO_2 could occur,³⁸ which consequently disfavors its formation according to eq 5 in Table 3. Such a hindrance became improved when the total pressure was increased above 0.1 MPa (Figure 5a), where the deviation of $\text{Cs}_2\text{SiO}_3(\text{s})$ from its normalized amount had been diminished. Despite its bulk formation, Cs_2SiO_3 had indicated its large dependence on steam partial pressure, cesium abundance (i.e., Cs/Al + Si), and total pressure to gain its stability in the Cs–Ca–Al–Si–O–H system, which therefore suggests its inferiority as compared to CsAlSiO_4 when rapid and unpredicted changes of atmospheric conditions have taken place.

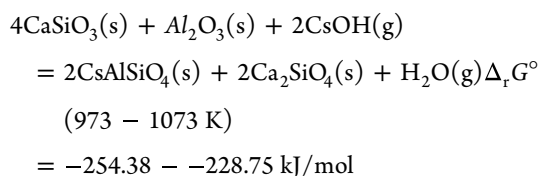
3.4. Implications to the Provenance of Cesium-Bearing Material. We have demonstrated in this study that cesium could chemically react with thermal insulation by forming cesium aluminum silicate (CsAlSiO_4) and dicalcium silicate (Ca_2SiO_4). These reaction products have been confirmed not only to be thermally stable but also water-insoluble in the scope of a 72 h water dissolution process.

While Cs_2SiO_3 was theoretically predicted to be present after such a reaction, it suffered water dissolution. Therefore, it can be inferred that the most stable cesium phase in a reaction system of Cs–Ca–Al–Si–O–H is CsAlSiO_4 . Our findings have shown experimentally and theoretically that even with only a fractional amount of aluminum in the thermal insulation, the formation of CsAlSiO_4 could occur. This means, e.g., in the event of a nuclear severe accident, that the location where radioactive cesium leaks and becomes exposed to Si(Al) materials would be a highly determining factor. In our study, we focused on the origin of Si(Al) materials as calcium silicate thermal insulation, which is based on its bulk use in the nuclear reactor piping system.¹⁷ Consequently, the point of encounter between calcium silicate thermal insulation and cesium was centered on any mechanical failure event associated with the piping system, for instance, at safety relief valves (SRVs). Despite no consensus concerning the leakage path of radioactive cesium in the Fukushima Daiichi nuclear power plant,^{39,40} several research institutes in the framework of the BSAF phase 2 project had predicted the potential SRV leak or failure, to resemble the actual pressure readings in the reactor and containment vessels during the accident. Therefore, in a conservative way, we assume that during the degradation of fuel in the reactor core of Fukushima Daiichi nuclear power plant, a substantial amount of high-pressure and high-temperature steam-containing cesium from the degraded fuels was leaked from SRV components, causing direct exposure to the adjacent thermal insulation of main steam piping and realizing cesium retention by the formation of cesium-bearing materials as CsAlSiO_4 . Because of the light-weight nature of the formed material (0.20–4.79 g/cm³; derived from $(m_{\text{s1}} - m_{\text{s0}})/V_1$ of 973 and 1073 K tests in Table 2), its release from the plant site in the event of hydrogen explosion⁴¹ becomes conceivable. Our candidate cesium-bearing material (CsAlSiO_4) is consistent with some recent field-observed water-insoluble cesium-bearing materials,^{8,42,43} where the coherent elemental distribution of Cs, O, Si, and Al was obtained. Nevertheless, due to the non-negligible incorporation of other constituents such as Fe and Zn in the materials, it is imperative to further investigate whether they originate from the field and hence contaminated the quantitative analyses reported in the works^{8,42,43} or they are intrinsic to the Si(Al)-material prior to reaction with cesium.

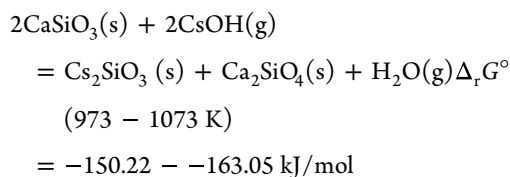
4. CONCLUSIONS

A simulated gaseous reaction of cesium with siliceous (calcium silicate) thermal insulation had been investigated at high temperature under the steam atmospheric condition to unveil the unprecedented cesium retention in the event of a nuclear severe accident. Three independent groups of tests were evaluated based on the reaction temperature of 873, 973, and 1073 K, respectively. The 973 and 1073 K tests were targeted to provide an understanding of the intended phenomenon involving the gas–solid reaction between cesium and thermal insulation, while the 873 K test was an extended case to anticipate a condition when gaseous cesium preceding its reaction with thermal insulation was condensed.

Based on the post-test analyses and thermodynamic evaluation, it was found that at 973 and 1073 K, the dehydrated thermal insulation material (i.e. $\text{Ca}_6\text{Si}_6\text{O}_{17}(\text{OH})_2(\text{s}) \rightarrow 6\text{CaSiO}_3(\text{s}) + \text{H}_2\text{O}(\text{g})$) reacted with cesium in the following two reactions:

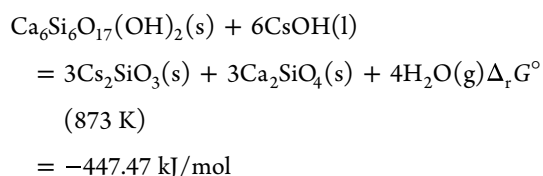


and



Large retention of cesium on the thermal insulation material ranging from 45 to 84 wt % initial insulator was observed in these groups of tests. It was comprehended that the majority of retained cesium prevailed as water-soluble Cs_2SiO_3 .

Meanwhile, at 873 K, where condensed phases reaction was expected to occur, it was found that the reaction occurred between the hydrated thermal insulation and cesium as



It was not possible to explicitly determine the amount of retained cesium that belongs to Cs_2SiO_3 in this group due to influences from unreacted $\text{CsOH}(\text{l})$. However, considering a proportion between Cs_2SiO_3 and Ca_2SiO_4 in the given reaction, an approximate amount of Cs_2SiO_3 could be estimated from the results of quantitative XRD on the sample with identified Ca_2SiO_4 such that in sample 3-2. With an amount of 49.7 wt % Ca_2SiO_4 , it was calculated that Cs_2SiO_3 could be formed ca. 98.7 wt %.

To this end, many debates arose about the provenance of Si(Al)-containing material be caused by framing the CsMP formation to be valid only on a single event rather than combined or multiple events. This seems plausible because at one time, the assumed formation could explain a portion of CsMP constituents but failed to explain the existence of others. Finally, our study does not rule out those hypotheses of CsMP formation (e.g., concrete origin⁵ and stainless steel origin¹³) due to the possible multiple events in nuclear accidents progression; instead, it provides a more realistic approach comprising gas–solid and/or condensed phases reaction, which could be experimentally validated.

■ ASSOCIATED CONTENT

SI Supporting Information

The Supporting Information is available free of charge at <https://pubs.acs.org/doi/10.1021/acsomega.2c03525>.

XRD results of the 1073 K test sample before and after water dissolution and the EDS elemental mapping on selected samples from each group of tests (PDF)

■ AUTHOR INFORMATION

Corresponding Author

Muhammad Rizaal – Nuclear Science and Engineering Center, Japan Atomic Energy Agency, Tokai-mura, Naka-gun, Ibaraki 319-1195, Japan; orcid.org/0000-0003-2198-2325; Email: rizaal.muhammad@jaea.go.jp

Authors

Kunihisa Nakajima – Nuclear Science and Engineering Center, Japan Atomic Energy Agency, Tokai-mura, Naka-gun, Ibaraki 319-1195, Japan

Takumi Saito – Nuclear Professional School, School of Engineering, The University of Tokyo, Tokai-mura, Naka-gun, Ibaraki 319-1188, Japan; orcid.org/0000-0002-4403-9607

Masahiko Osaka – Nuclear Science and Engineering Center, Japan Atomic Energy Agency, Tokai-mura, Naka-gun, Ibaraki 319-1195, Japan

Koji Okamoto – Nuclear Professional School, School of Engineering, The University of Tokyo, Tokai-mura, Naka-gun, Ibaraki 319-1188, Japan

Complete contact information is available at:

<https://pubs.acs.org/10.1021/acsomega.2c03525>

Notes

The authors declare no competing financial interest.

■ REFERENCES

- (1) Adachi, K.; Kajino, M.; Zaizen, Y.; Igarashi, Y. Emission of spherical cesium-bearing particles from an early stage of the Fukushima nuclear accident. *Sci. Rep.* **2013**, *3*, 2554.
- (2) Igarashi, Y.; Kogure, T.; Kurihara, Y.; Miura, H.; Okumura, T.; Satou, Y.; Takahashi, Y.; Yamaguchi, N. A Review of Cs-bearing microparticles in the environment emitted by the Fukushima Dai-Ichi nuclear power plant accident. *J. Environ. Radioact.* **2019**, *205–206*, 101–118.
- (3) Satou, Y.; Sueki, K.; Sasa, K.; Adachi, K.; Igarashi, Y. First successful isolation of radioactive particles from soil near the Fukushima Daiichi nuclear power plant. *Anthropocene* **2016**, *14*, 71–76.
- (4) Satou, Y.; Sueki, K.; Sasa, K.; Yoshikawa, H.; Nakama, S.; Minowa, H.; Abe, Y.; Nakai, I.; Ono, T.; Adachi, K.; Igarashi, Y. Analysis of two forms of radioactive particles emitted during the early stages of the Fukushima Dai-Ichi nuclear power station accident. *Geochem. J.* **2018**, *52*, 137–143.
- (5) Furuki, G.; Imoto, J.; Ochiai, A.; Yamasaki, S.; Nanba, K.; Ohnuki, T.; Grambow, B.; Ewing, R. C.; Utsunomiya, S. Caesium-rich micro-particles: A window into the meltdown events at the Fukushima Daiichi nuclear power plant. *Sci. Rep.* **2017**, *7*, 42731.
- (6) Ono, T.; Iizawa, Y.; Abe, Y.; Nakai, I.; Terada, Y.; Satou, Y.; Sueki, K.; Adachi, K.; Igarashi, Y. Investigation of the chemical characteristics of individual radioactive microparticles emitted from reactor 1 by the Fukushima Daiichi nuclear power plant accident by using multiple synchrotron radiation X-ray analyses. *Bunseki Kagaku* **2017**, *66*, 251–261.
- (7) Ikehara, R.; Suetake, M.; Komiyama, T.; Furuki, G.; Ochiai, A.; Yamasaki, S.; Bower, W. R.; Law, G. T. W.; Ohnuki, T.; Grambow, B.; Ewing, R. C.; Utsunomiya, S. Novel method of quantifying radioactive cesium-rich microparticles (CsMPs) in the environment from the Fukushima Daiichi nuclear power plant. *Environ. Sci. Technol.* **2018**, *52*, 6390–6398.
- (8) Yamaguchi, N.; Kogure, T.; Mukai, H.; Akiyama-Hasegawa, K.; Mitome, M.; Hara, T.; Fujiwara, H. Structures of radioactive Cs-bearing microparticles in non-spherical forms collected in Fukushima. *Geochem. J.* **2018**, *52*, 123–136.

- (9) Yamaguchi, N.; Mitome, M.; Kotone, A.-H.; Asano, M.; Adachi, K.; Kogure, T. Internal structure of cesium-bearing radioactive microparticles released from Fukushima nuclear power plant. *Sci. Rep.* **2016**, *6*, 20548.
- (10) Kogure, T.; Yamaguchi, N.; Segawa, H.; Mukai, H.; Motai, S.; Akiyama-Hasegawa, K.; Mitome, M.; Hara, T.; Yaita, T. Constituent elements and their distribution in the radioactive Cs-bearing silicate glass microparticles released from Fukushima nuclear plant. *Microscopy* **2016**, *65*, 451–459.
- (11) Miura, H.; Kurihara, Y.; Sakaguchi, A.; Tanaka, K.; Yamaguchi, N.; Higaki, S.; Takahashi, Y. Discovery of radiocesium-bearing microparticles in river water and their influence on the solid-water distribution coefficient (K_d) of radiocesium in the Kuchibuto River in Fukushima. *Geochem. J.* **2018**, *52*, 145–154.
- (12) Nishihara, K.; Iwamoto, H.; Suyama, K. *Estimation of fuel compositions in Fukushima-Daiichi nuclear power plant*; JAEA-Data/Code 2012–018; Japan Atomic Energy Agency: Ibaraki, Japan, 2012.
- (13) Zheng, L.; Hosoi, K.; Ueda, S.; Gao, X.; Kitamura, S.; Kobayashi, Y. Si-rich phases and their distributions in the oxide scale formed on 304 stainless steel at high temperatures. *J. Nucl. Mater.* **2018**, *507*, 327–338.
- (14) Martin, P. G.; Satou, Y.; Griffiths, I.; Richards, D.; Scott, T. Analysis of external surface irregularities on Fukushima-derived fallout particles. *Front. Energy Res.* **2017**, *5*, 25.
- (15) Rizaal, M.; Nakajima, K.; Saito, T.; Osaka, M.; Okamoto, K. Investigation of high-temperature chemical interaction of calcium silicate insulation and cesium hydroxide. *J. Nucl. Sci. Technol.* **2020**, *57*, 1062–1073.
- (16) Osborne, M. F.; Collins, J. L.; Lorenz, R. A. Experimental studies of fission product release from commercial light water reactor fuel under accident conditions. *Nucl. Technol.* **1987**, *78*, 157–169.
- (17) Nuclear and Industrial Safety Agency. *Report on emergency core cooling system strainer and containment vessel recirculation sump screen blocking event and status of measures on boiling water nuclear power plant*; 44th Nuclear Safety Commission Report material no. 2 [in Japanese]; Nuclear and Industrial Safety Agency (NISA): Tokyo, Japan, 2006.
- (18) Andersson, J.-O.; Helander, T.; Höglund, L.; Shi, P.; Sundman, B. THERMO-CALC & DICTRA, Computational tools for materials science. *Calphad* **2002**, *26*, 273–312.
- (19) Yui, K.; Kuramochi, H.; Osako, M. Understanding the behavior of radioactive cesium during the incineration of contaminated municipal solid waste and sewage sludge by thermodynamic equilibrium calculation. *ACS Omega* **2018**, *3*, 15086–15099.
- (20) Lindemer, T. B.; Besmann, T. M.; Johnson, C. E. Thermodynamic review and calculations –alkali-metal oxide systems with nuclear fuels, fission products, and structural materials. *J. Nucl. Mater.* **1981**, *100*, 178–226.
- (21) Taylor, P.; DeVaal, S. D.; Owen, D. G. Stability relationships between solid cesium aluminosilicates in aqueous solutions at 200 °C. *Can. J. Chem.* **1989**, *67*, 76–81.
- (22) Ogorodova, L. P.; Melchakova, L. V.; Kiseleva, I. A.; Belitsky, I. A. Thermochemical study of natural pollucite. *Thermochim. Acta* **2003**, *403*, 251–256.
- (23) Dent, L. S.; Taylor, H. F. W. The dehydration of xonotlite. *Acta Cryst.* **1956**, *9*, 1002–1004.
- (24) Cordfunke, E. H. P.; Konings, R. J. M. M. The Cs-O-H System. In *Thermochemical data for reactor materials and fission products*; Cordfunke, E. H. P.; Konings, R. J. M. M., Eds.; Elsevier Science Publishers B. V.: Amsterdam, 1990; pp. 103–109, ISBN 0–444–88485-8.
- (25) Doebelin, N.; Kleeberg, R. Profex: A graphical user interface for the rietveld refinement program BGMN. *J. Appl. Crystallogr.* **2015**, *48*, 1573–1580.
- (26) Shaw, S.; Henderson, C. M. B.; Komanschek, B. U. Dehydration/recrystallization mechanisms, energetics, and kinetics of hydrated calcium silicate minerals: An in situ TGA/DSC and synchrotron radiation SAXS/WAXS study. *Chem. Geol.* **2000**, *167*, 141–159.
- (27) Geng, G.; Myers, R. J.; Qomi, M. J. A.; Monteiro, P. J. M. Densification of the interlayer spacing governs the nanomechanical properties of calcium-silicate-hydrate. *Sci. Rep.* **2017**, *7*, 1–8.
- (28) Pegado, L.; Labbez, C.; Churakov, S. V. Mechanism of aluminium incorporation into C-S-H from Ab initio calculations. *J. Mater. Chem. A* **2014**, *2*, 3477–3483.
- (29) Kunhi Mohamed, A.; Moutzouri, P.; Berruyer, P.; Walder, B. J.; Siramanont, J.; Harris, M.; Negroni, M.; Galmarini, S. C.; Parker, S. C.; Scrivener, K. L.; Emsley, L.; Bowen, P. The atomic-level structure of cementitious calcium aluminate silicate hydrate. *J. Am. Chem. Soc.* **2020**, *142*, 11060–11071.
- (30) Ishida, H.; Mabuchi, K.; Sasaki, K.; Mitsuda, T. Low-temperature synthesis of β -Ca₂SiO₄ from Hillebrandite. *J. Am. Ceram. Soc.* **1992**, *75*, 2427–2432.
- (31) Rizaal, M.; Nakajima, K.; Saito, T.; Osaka, M.; Okamoto, K. *Determination of soluble Cs compound formed at high temperature in the system of Cs₂O-CaO-SiO₂*; Unpublished research, 2022.
- (32) Spencer, P. J. *The thermodynamic properties of silicates*; NPL Report Chemistry 21; National Physical Laboratory (NPL): London, United Kingdom, 1973.
- (33) Ball, R. G. J.; Bowsher, B. R.; Cordfunke, E. H. P.; Dickinson, S.; Konings, R. J. M. Thermochemistry of selected fission product compounds. *J. Nucl. Mater.* **1993**, *201*, 81–91.
- (34) Hoch, C.; Röhr, C. Alkalimetall-Oxosilicate A₆[Si₃O₉] und A₆[Si₂O₇] (A = Rb, Cs): Darstellung und Kristallstruktur. *Z. Naturforsch., B* **2001**, *56*, 423–430.
- (35) Zheng, Q.; Wang, W. Calcium silicate based high efficiency thermal insulation. *Br. Ceram. Trans.* **2000**, *99*, 187–190.
- (36) Black, L.; Garbev, K.; Stumm, A. Structure, bonding and morphology of hydrothermally synthesised xonotlite. *Adv. Appl. Ceram.* **2009**, *108*, 137–144.
- (37) Milestone, N. B.; Ahari, G. K. Hydrothermal processing of Xonotlite based compositions. *Adv. Appl. Ceram.* **2007**, *106*, 302–308.
- (38) Stolyarova, V. L.; Lopatin, S. I.; Belousova, O. L.; Grishchenko, L. V. Phase equilibria and thermodynamic properties of components in the Cs₂O-B₂O₃-SiO₂ system at high Temperatures. *Glass Phys. Chem.* **2006**, *32*, 55–62.
- (39) Herranz, L. E.; Pellegrini, M.; Lind, T.; Sonnenkalb, M.; Godin-Jacquin, L.; López, C.; Dolganov, K.; Cousin, F.; Tamaki, H.; Kim, T. W.; Hoshi, H.; Andrews, N.; Sevon, T. Overview and outcomes of the OECD/NEA benchmark study of the accident at the Fukushima Daiichi NPS (BSAF) Phase 2 – Results of severe accident analyses for Unit 1. *Nucl. Eng. Des.* **2020**, *369*, No. 110849.
- (40) Sonnenkalb, M.; Pellegrini, M.; Herranz, L. E.; Lind, T.; Morreale, A. C.; Kanda, K.; Tamaki, H.; Kim, S. I.; Cousin, F.; Fernandez Moguel, L.; Andrews, N.; Sevon, T. Overview and outcomes of the OECD/NEA benchmark study of the accident at the Fukushima Daiichi NPS (BSAF) Phase 2 – Results of severe accident analyses for Unit 2. *Nucl. Eng. Des.* **2020**, *369*, No. 110840.
- (41) Tokyo Electric Power Company. *Evaluation of the situation of cores and containment vessels of Fukushima Daiichi nuclear power station units-1 to 3 and examination into unsolved issues in the accident progression*; Progress report no. 5; Tokyo Electric Power Company (TEPCO): Tokyo, Japan, 2017.
- (42) Futagami, F.; Soliman, M.; Takamiya, K.; Sekimoto, S.; Oki, Y.; Kubota, T.; Konno, M.; Mizuno, S.; Ohtsuki, T. Isolation, characterization and source analysis of radiocaesium micro-particles in soil sample collected from vicinity of Fukushima Dai-ichi nuclear power plant. *J. Environ. Radioact.* **2020**, *223-224*, No. 106388.
- (43) Fueda, K.; Takami, R.; Minomo, K.; Morooka, K.; Horie, K.; Takehara, M.; Yamasaki, S.; Saito, T.; Shiotsu, H.; Ohnuki, T.; Law, G. T. W.; Grambow, B.; Ewing, R. C.; Utsunomiya, S. Volatilization of B₄C control rods in Fukushima Daiichi nuclear reactors during meltdown: B–Li isotopic signatures in cesium-rich microparticles. *J. Hazard. Mater.* **2022**, *428*, No. 128214.